ELSEVIER

Journal of Fluids and Structures 24 (2008) 1278–1283

JOURNAL OF FLUIDS AND STRUCTURES

www.elsevier.com/locate/jfs

Control of vortex breakdown in a closed cylinder with a small rotating rod

D. Lo Jacono[a,*], J.N. Sørensen[b], M.C. Thompson[a,c], K. Hourigan[a,c]

[a]*Department of Mechanical and Aerospace Engineering, Monash University, 3800 Melbourne, Australia*
[b]*Department of Mechanical Engineering, Technical University of Denmark, 2800 Lyngby, Denmark*
[c]*Division of Biological Engineering, Monash University, 3800 Melbourne, Australia*

Received 30 January 2008; accepted 26 June 2008
Available online 22 October 2008

Abstract

Effective control of vortex breakdown in a cylinder with a rotating lid was achieved with small rotating rods positioned on the stationary lid. After validation with accurate measurements using a novel stereoscopic particle image velocimetry (SPIV) technique, analysis of numerical simulations using a high-order spectral element method has been undertaken. The effect of a finite length rod creates additional source terms of vorticity as the rod rotates. These additional source terms and their spatial locations influence the occurrence of the vortex breakdown.

Keywords: Vortex breakdown; Control; SPIV

1. Introduction

The flow within a closed cylinder with a rotating lid is considered. This type of flow has been the focus of earlier studies involving vortex breakdown, including relevance to bioreactor design, see for example Vogel (1968), Escudier (1984), Lopez (1990), Sørensen and Christensen (1995), Spohn et al. (1998), Özögren et al. (2002), Dusting et al. (2006). However, vortex breakdown is not fully understood and remains difficult to predict and control. Recently, there have been attempts to control this phenomenon. Husain et al. (2003) studied the addition of a rotating axial rod and Herrada and Shtern (2003) investigated the introduction of temperature gradients. Mununga et al. (2004) studied the effect of a small rotating disk opposite to the driving lid. In this study, we propose to determine the effect on vortex breakdown of a small rotating rod positioned along the centre axis. This will bridge the gap in knowledge between the two limiting cases (i.e., that of a rotating disc and of a full length rotating rod) studied previously. Experimental results undertaken in the cylindrical cavity will be presented for the axial rotating rod and for the partial rotating rod for several rotating configurations. In addition to these experiments, high order numerical simulations have been performed in order to provide additional accuracy, especially in the immediate neighbourhood of the rod allowing results to be further interpreted.

*Corresponding author.
E-mail address: david.lojacono@eng.monash.edu.au (D. Lo Jacono).

0889-9746/$ - see front matter © 2008 Elsevier Ltd. All rights reserved.
doi:10.1016/j.jfluidstructs.2008.06.015

2. Experimental set-up

The experimental set-up consists of a cylinder of diameter $D \equiv 2R = 65\,\text{mm}$ that was filled with water and placed in the centre of an octagonal shaped container, see Fig. 1. The octagonal shape allows the exterior faces of the rig to be flat in order to reduce refraction effects that result in optical distortion errors during the use of image-based measurement techniques. A flat, circular disk acted as the rotating bottom, and was located in the centre of the base. The rod diameter used here was fixed to be $d = 3\,\text{mm}$, and acted as the control device. For the partial rod experiments, an $l = 13\,\text{mm}$ height rod was used ($\lambda = l/R = 0.4$, where λ is the dimensionless length of the control device). The shafts of the disk and the rod were rotated by two independent small stepper motors via a high-performance motion controller. Stereoscopic particle image velocimetry (SPIV) was the primary tool used for quantitative flow measurement. A brief outline of the apparatus is given below; a more general description of the method used can be found in Fouras et al. (2008). An angular displacement system was chosen, meaning that the two CCD cameras (PCO Imaging Pixelfly) were positioned at a fixed angle off center. Calibration was conducted using the third camera located normal to the laser sheet. The tracer particles used were silver coated hollow glass micro-spheres with a nominal diameter of 12 μm and were illuminated by a 1.0 mm thick light sheet powered by the 532 nm laser.

3. Computational method

The incompressible Navier–Stokes equations were solved using a spectral-element technique. The simulations were undertaken on a 400 macro-element mesh carefully concentrated towards the solid boundaries. Within each mesh cell macro element, the velocity and pressure fields were represented by seventh-order tensor-product polynomials, after initial testing indicated that this was sufficient resolution to provide grid independent results. Details of this approach and implementation can be found in Thompson et al. (1996). Axisymmetry and no-slip boundary conditions were applied on the appropriate sides of the computational domain.

4. Results and discussion

The parameters governing the flow consist of the aspect ratio of the rig $H/R = 1.85$ which is kept constant, the Reynolds number $\text{Re} = \omega_{\text{lid}} R^2/\nu$, where ω_{lid} is the angular speed of the driving lid and ν is the kinematic viscosity of the fluid, and the ratio between the two Reynolds numbers $\gamma = (\omega_{\text{rod}} r^2)/(\omega_{\text{lid}} R^2)$. All variables are made dimensionless using R and ω_{lid} as reference scales. All experimental data are non-dimensionalised with the previously defined characteristic scales to allow direct comparison with numerical results. The Reynolds number is kept constant and equal to 2 200, and our main control parameter will be γ. It should be mentioned that for the selected parameters (aspect ratio and Reynolds number), the regime is expected to be laminar and steady. The measurements confirmed this and accordingly, we were able to time-average several PIV-snapshots (≈ 100) for each camera. The computations also confirmed the laminar and steady state of the flow for these given parameters and the code was stopped after convergence of the velocity field ($\approx 10^{-8}$ for each field).

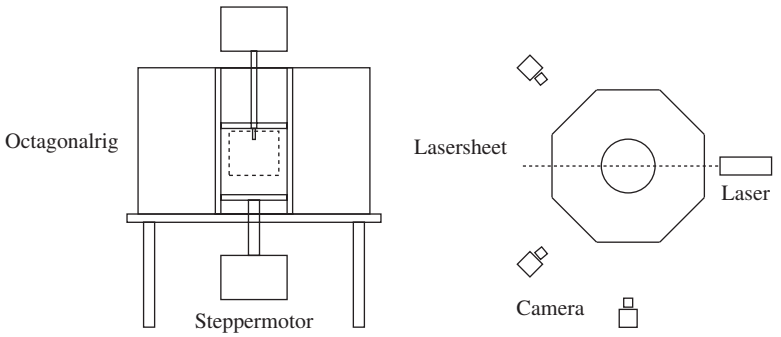

Fig. 1. Experimental apparatus, here shown with a partial axial rod. Left: vertical cross-section, where the dotted window represents the SPIV-field. Right: Top view and SPIV set-up.

Fig. 2 shows the effect of a thin rod undergoing co-rotation and counter-rotation, respectively. These figures represent iso-contours of the axial velocity, and of interest is the zero value contour (solid line) delimiting the vortex breakdown. The additional swirl provided by the axial rod on the vortex breakdown is striking. For co-rotation ($\gamma > 0$) the vortex breakdown diminishes and even vanishes with increasing γ. However, for counter-rotation, the effect is the opposite; the vortex breakdown increases in size and a second breakdown appears for decreasing γ. This variation of vortex breakdown with γ is qualitatively consistent with previous published work of Husain et al. (2003).

This introduction of a rotating rod will generate additional axial vorticity near the lid. The azimuthal vorticity component equation can be written in cylindrical coordinates (r, θ, z) as follows:

$$\frac{\partial \omega}{\partial t} = -\frac{\partial}{\partial r}(u_r \omega) - \frac{\partial}{\partial z}(u_z \omega) + \frac{1}{r}\frac{\partial}{\partial z}(u_\theta^2) + \frac{1}{\mathrm{Re}}\left[\frac{\partial}{\partial r}\left(\frac{1}{r}\frac{\partial r\omega}{\partial r}\right) + \frac{\partial^2 \omega}{\partial z^2}\right], \tag{1}$$

where the azimuthal vorticity is $\omega = (\boldsymbol{\nabla} \times \boldsymbol{u}) \cdot \boldsymbol{e}_\theta$, the flow velocity $\boldsymbol{u} = (u_r, u_\theta, u_z)$ and $\boldsymbol{e}_\theta$ is the azimuthal unit vector. For a rod running throughout the cylinder, one significant way the rotational motion introduced by the rod can affect the vorticity, influencing in turn the flow behaviour in the meridional plane, is through the source term:

$$S = \frac{1}{r}\frac{\partial u_\theta^2}{\partial z}. \tag{2}$$

At the curved surface of the rotating rod, the source term is null (u_θ does not vary with z). Away from the rod, the source term is expected not to have a significant effect on the flow as the azimuthal velocity introduced by the rotating rod is mainly a function of r. However, close to the rod and especially near the lid, the azimuthal velocity experiences a jump from the constant rotating speed of the rod and the surrounding flow. This source term will generate a velocity field according to the Biot–Savart induction law.

In order to investigate the physics underlying the mechanism, additional experiments have been undertaken. The full axial rod used by Husain et al. (2003) has been replaced with the partial thin axial rod ($\lambda = 0.4$). It was verified that the introduction of a small *non-rotating* rod has no significant effect on the flow into which it is introduced. In these types of flow, it has been found that even the slightest imperfections in the apparatus will create asymmetries (Thompson and Hourigan, 2003). However, the authors wish to stress that although the measurements presented asymmetrical fields, these fields were steady in time allowing the average of the subsequent PIV-snapshots. Furthermore, the asymmetry that could be observed could have several sources such as minor imperfection in the rig (Thompson and Hourigan, 2003;

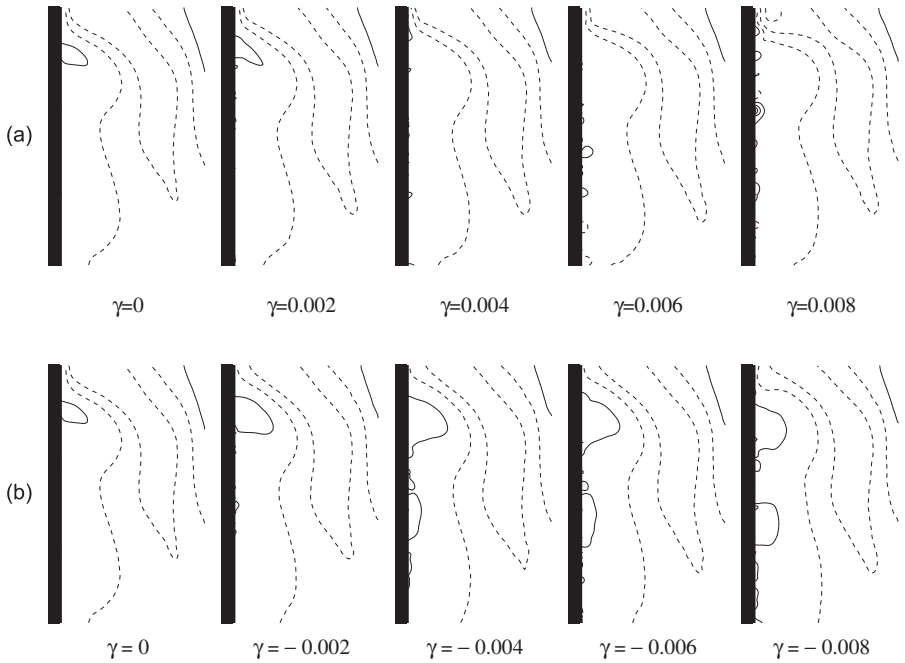

Fig. 2. Top (bottom) row presents the effect of a co-(counter-)rotating thin rod Re = 2 200. Only the axial velocity is shown for several rotational speeds. Solid and dashed lines represent zero and negative axial velocities, respectively.

Brøns et al., 2007), the orientation of the camera/lens, the laser sheet position and orientation. Nevertheless, bearing these experimental complications in mind the authors believe that the experimental results were of good quality. In short, from the individual PIV-snapshots, it was deduced the flow did not present any measurable helical structures that precess around the vortex centreline. Thompson and Hourigan (2003) and others have observed and predicted a steady asymmetric bubble. In order to validate against an axisymmetric CFD simulation, flow measurements have been averaged over the two half planes to produce symmetric data.

Fig. 3 shows the comparison of matched iso-contours for the velocity components between symmetric experimental data (in the boxed region) and numerical data (in the surrounding region) for the non-rotating ($\gamma = 0.0$), co-rotating ($\gamma = 0.01$) and counter-rotating ($\gamma = -0.01$) small rod cases, respectively. Note the excellent agreement between the numerical and the experimental data. It should be recalled that there is no smoothing or filtering of the experimental data from the SPIV process.

By inserting a small rotating rod, the recirculation region has been modified. But unlike the case of the full axial rod, co- or counter-rotating the short rod does not affect the bubble in the same fashion. This may be due to two different reasons: first, near the rotating lid and the long thin rod (at $z = 0$), there was a source term which does not appear with a short rod; second, near the edge at the free end of the small rod (at $z \approx 1.45$), a source term arising from the radial velocity developed at the edge of the rotating rod appears. This complicates the physical phenomena occurring with the recirculation bubble.

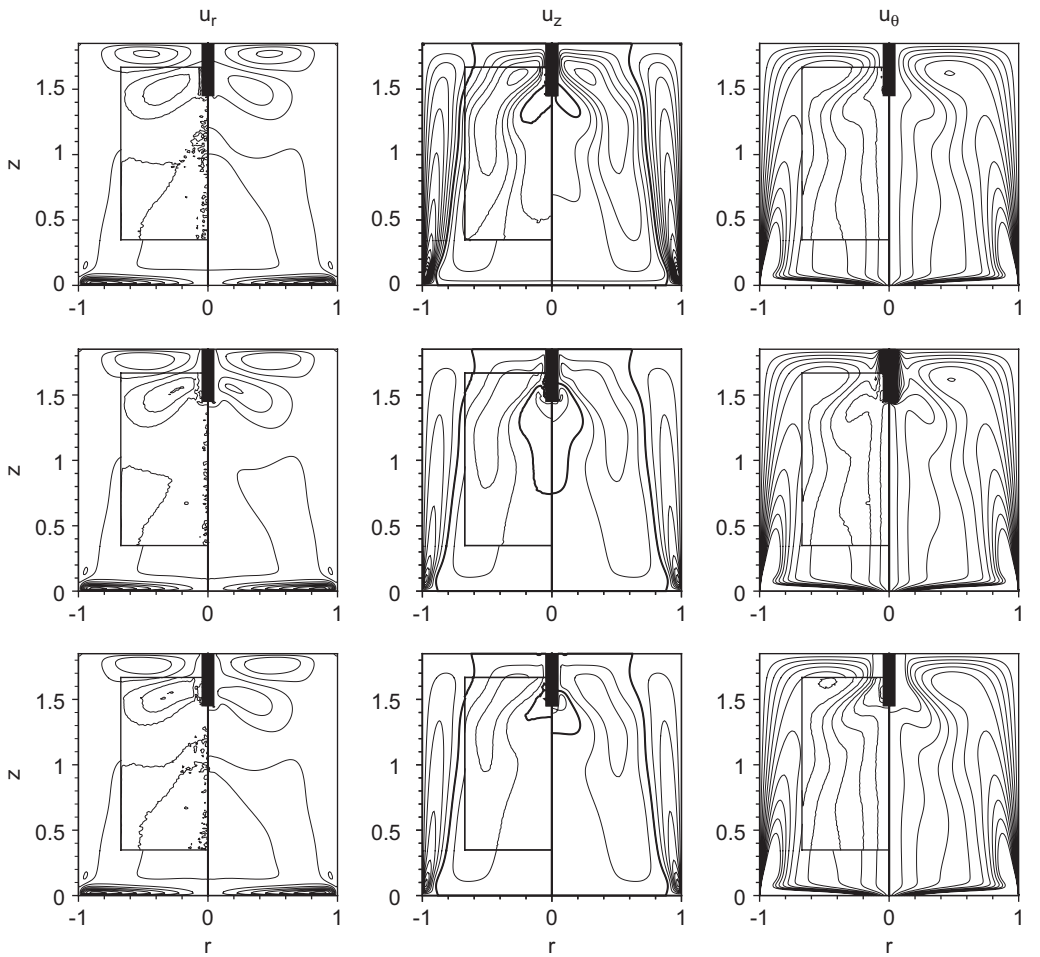

Fig. 3. Comparison of velocity iso-contours of the SPIV results at Re = 2200 and $H/R = 1.85$, with numerical simulations, for a thin partial rod ($\lambda = 0.4$). Top row: the rod is not rotating, $\gamma = 0.0$. Middle row: the rod rotation is set to $\gamma = 0.1$. Bottom row: the rod rotation is set to $\gamma = -0.1$. The experimental iso-contours region are shown in the window at the left hand side of each image and are surrounded by the numerical iso-contours.

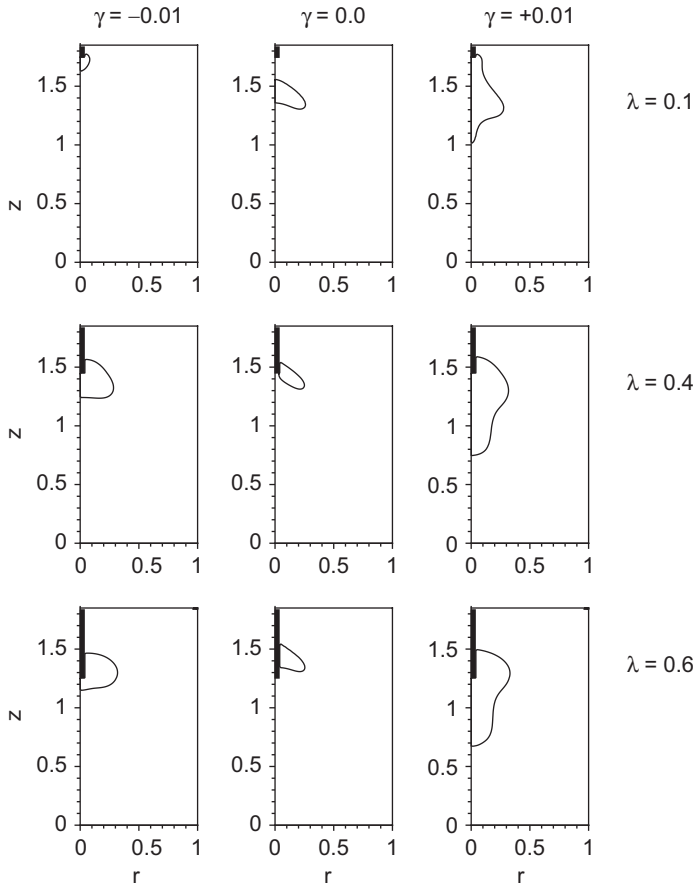

Fig. 4. Numerical simulations performed for several rod lengths. The iso-contour represented is the zero-streamline, in other words the boundary of the recirculation zone.

Fig. 4 shows the results of varying the length of the rod on the recirculation zone. Three different rod lengths, λ, with three different rotating ratios, γ, are presented. These numerical simulations display the zero valued streamline, outlining the recirculation bubble. The simulations for the non-rotating case ($\gamma = 0$) show that the introduction of a stationary rod does not affect the recirculation zone. If the length of the control device approaches zero, the direction of rotation has more impact on the recirculation zone. For co-rotational values, the recirculation zone undergoes an expansion, whereas for counter-rotational values the zone contracts. For longer rods, the pattern of the recirculation zone changes little with the rotational direction. As the length of the control device increases further, this behaviour will change as one can observe for the full length rod experiments. It is expected that the transition point in behaviour will occur for rod length close to full-length. For small values of λ, it can be argued that as the rod shortens it approaches the shape of a flat disk on the upper lid ($\lambda \to 0$). As observed, the recirculation zone disappears for counter-rotation. This result is similar to that of Mununga et al. (2004), where a disk flush with the upper-lid was rotating.

5. Conclusions

The effect of the presence of a finite width full and short rod on the vortex breakdown in a confined cylindrical cavity has been investigated by means of experiments and numerical simulation. The measured experimental velocity field and numerical simulation are in good agreement. For a long axial rod, it was confirmed that the co-rotation suppresses the vortex breakdown, unlike counter-rotation which enhances the vortex breakdown region. For short rod length,

additional vorticity source terms complicate the behaviour of the recirculation zone when the rod rotates. As the rod shortens, the breakdown behaviour approaches the limit of a flat disk and the recirculation bubble vanishes for sufficient counter-rotational speed.

Acknowledgements

D.L. thanks the Swiss National Science Foundation for their support. The authors are grateful for support from the Australian Research Council under Discovery Grant DP0452664 and Linkage International Grant LX0668992.

References

Brøns, M., Shen, W.Z., Sørensen, J.N., Zhu, W.J., 2007. The influence of imperfections on the flow structure of steady vortex breakdown bubbles. Journal of Fluid Mechanics 578, 453–466.

Dusting, J., Sheridan, J., Hourigan, K., 2006. A fluid dynamics approach to bioreactor design for cell and tissue culture. Biotechnology and Bioengineering 94 (6).

Escudier, M., 1984. Observations of the flow produced in a cylindrical container by a rotating endwall. Experiments in Fluids 2, 189–196.

Fouras, A., Lo Jacono, D., Hourigan, K., 2008. Target-free stereo PIV: a novel technique with inherent error estimation and improved accuracy. Experiments in Fluids 44 (2), 317–329.

Herrada, M., Shtern, V., 2003. Control of vortex breakdown by temperature gradients. Physics of Fluids 15, 3468–3477.

Husain, H., Shtern, V., Hussain, F., 2003. Control of vortex breakdown by addition of near-axis swirl. Physics of Fluids 15, 271–279.

Lopez, J., 1990. Axisymmetrical vortex breakdown. Part 1. Confined swirling flow. Journal of Fluid Mechanics 221, 533–552.

Mununga, L., Hourigan, K., Thompson, M., Leweke, T., 2004. Confined flow vortex breakdown control using a small rotating disk. Physics of Fluids 16, 4750–4753.

Özögren, M., Sahin, B., Rockwell, D., 2002. Vortex breakdown from a pitching delta wing incident upon a plate: flow structure as the origin of buffet loading. Journal of Fluids and Structures 16 (3), 295–316.

Sørensen, J., Christensen, E., 1995. Direct numerical simulation of rotating fluid-flow in a closed cylinder. Physics of Fluids 7, 764–778.

Spohn, A., Mory, M., Hopfinger, E., 1998. Experiments on vortex breakdown in a confined flow generated by rotating disk. Journal of Fluid Mechanics 370, 73–99.

Thompson, M., Hourigan, K., 2003. The sensitivity of steady vortex breakdown bubbles in confined cylinder flows to rotating lid misalignment. Journal of Fluid Mechanics 496, 129–138.

Thompson, M., Hourigan, K., Sheridan, J., 1996. Three-dimensional instabilities in the wake of a circular cylinder. Experimental Thermal and Fluid Science 12, 190–196.

Vogel, H., 1968. Experimentelle ergebnisse über die laminare strömung in einem zylindrischen gehäuse mit darin rotierender scheibe. Bericht 6, Max–Planck-Institut für Strömungdforschung, Göttingen.